SBIR/STTR RIGHTS NOTICE

These SBIR/STTR data are furnished with SBIR/STTR rights under Grant No. DE-FG02-06ER84560. For a period of 4 years after acceptance of all items to be delivered under this grant, the government agrees to use these data for Government purposes only, and they shall not be discussed outside the Government (including disclosure for procurement purposes) during such period without the permission of the grantee, except that, subject to the forgoing use and disclosure prohibitions, such data may be disclosed for use by support contractors. After the aforesaid 4-year period the Government has a royalty-free license to use, and to authorize others to use on its behalf, these data for Government purpose, but is relived of all disclosure prohibitions and assumes no liability for unauthorized use of these data by third parties. This notice shall be affixed to any reproductions of these data in whole or in part.

A New Class of Creep Resistant Oxide/Oxide Ceramic Matrix Composites

FINAL REPORT

Contract No: DE-FG02-06ER84560
Contract Period: 7/01/06-3/31/07
NEI Project Code: NEI43047

NEI Corporation
400E Apgar Drive
Somerset, NJ 08873
Ph: (732) 868-3141
www.neicorporation.com

Principal Investigator: Dr. Mohit Jain
Dr. Ganesh Skandan
Prof. Roger Cannon, Rutgers University

A. INTRODUCTION

With the development of SiC-SiC fiber-reinforced composites in the last decade, hot sections of power generation gas turbines, including blades, nozzles, vanes, rotors, shrouds, combustor inner liners, and turbine rear frames, can now be fabricated out of ceramic matrix composites (CMCs), thereby enabling higher temperature of operation than is possible with Ni-base superalloys. When used with an environmental barrier coating (EBC), these *non-oxide* CMCs can lead to increased operating efficiency and lower levels of NO_x, CO_2 and hydrocarbons. On the other hand, *oxide fiber-reinforced oxide-matrix* CMCs are stable to the environment, and have the potential for longer lifetime and lower cost. However, high temperature mechanical properties, particularly creep strength, have limited the potential of oxide-based CMCs, most of which to date have been based on an aluminum oxide (Al_2O_3) matrix. The Phase I program has demonstrated that it is possible to overcome this barrier by developing a highly creep resistant yttrium aluminum garnet $Y_3Al_5O_{12}$ (YAG) based matrix.

The premise of the Phase I program was that "new and previously unexplored microstructures for the YAG matrix are needed to meet the stringent requirements of the high temperature environment in a gas turbine". To this end, there were two significant innovations in the Phase I program, which are summarized below in brief and explained in detail in Section D:

Reduction in high temperature creep rate by use of dopants

The introduction of a small concentration of dopant ions in the YAG powders during powder synthesis led to the segregation of dopant oxide at the grain boundaries in the sintered material (supported by data on lattice parameter). This in turn reduced the creep rate in the doped material by more than an order of magnitude compared to pure YAG. In fact, extrapolating high temperature compressive creep data to 1100 ^oC showed that the fully dense doped YAG is ~ two orders of magnitude more creep resistant than Nextel 720, which is the most creep resistant oxide fiber available commercially: 1×10^{-12} sec^{-1} vs. 1×10^{-10} sec^{-1} for the fiber at 75 MPa. Even after adjusting for reduced grain size and porosity in a practical CMC component, the creep rate in the doped YAG is about half an order of magnitude lower than that of the fiber. This is a particularly significant finding for two reasons: one, as explained below in detail, the lifetime of a CMC can be substantially enhanced by utilizing a matrix that has better creep resistance than the fiber; second, the matrix material developed in this program can be combined with developmental fibers that have even higher creep resistance than the commercial available Nextel series so that the state of the art in oxide/oxide CMCs can be advanced further.

Use of nanoparticles to obtain fully dense materials with a relatively large grain size

Although in practice, an oxide CMC matrix will not be more than 80% dense, it was imperative to use a fully dense material for test purposes so that reliable creep measurements could be obtained. To enable this, a high surface area nanoparticulate and deliberately aggregated YAG powder (both doped and undoped) was synthesized in-house and used as starting material. At a sintering temperature of 1700 ^oC and a modest external pressure of 24 MPa, a fully dense material with a grain size just under 10 μm was obtained. In fact, as intended, there was evidence of exaggerated grain growth in the sintered material. It is interesting to note that contrary to the conventional wisdom of using nanoparticles as starting material in order to obtain a fine-grained material, we used a highly aggregated but nanoparticulate starting powder to aid rapid and abnormal grain growth. This is important since the greater the grain size, the greater the creep resistance is. Sintering the YAG powder at a much lower temperature of 1300 ^oC gave rise to densities of ~ 70% and a grain size of ~ 2 μm. This shows the potential for obtaining high matrix densities in a CMC component at a temperature where the fiber will not be "damaged".

Following is the technical background, followed by a synopsis of the experimental work that was performed during the course of the Phase I program:

B. Technical Background

B.1 Background on Fiber-reinforced Composites

Since the mid-1990's CMCs rather than monolithic ceramics have been targeted for insertion into turbine engines and particularly as the material of choice for combustor liners. Beginning in the late-1990's long term testing of gas turbine CMC combustor liners began in earnest. By the end of 2006, Solar Turbines had accumulated >85,000 total hours of field testing of turbine engines with CMC combustor linings[1]. Most of the tests used SiC-SiC composites. These tests revealed that the major materials challenge to long term operation of SiC-SiC was volatilization of the silica protective layer by reaction with H_2O to form $Si(OH)_4$, leading to recession of liner thickness. In one early field test of uncoated CVI SiC-SiC composites by Solar Turbines, 80% of the wall thickness was lost in the hottest spot of the combustor. As a response to this problem environmental barrier coatings (EBC) are now applied and have been successful in decreasing the recession rate by a factor of two to three times. Commonly, three layer BSAS (barium strontium silicate)/mullite/Si coatings are applied. The purpose of the Si coating is to getter the final amount of oxygen making its way through the top two layers, and the mullite prevents the silica from reacting with the BSAS layer. Lifetime is not only limited by recession of the EBC by vaporization but also by the accumulation of silica in the inner coating which leads to spalling and ultimately limits the life of the EBCs. The best SiC-SiC composite combustor liners have so far endured ~15,000 hours. The goal is 30,000 hours for mid-size and large turbine generators.

Although recession due to volatilization is the major problem, it is reduction in the mechanical properties due to the damage which ultimately limits the lifetime of the combustor liners. One analysis considers recession to 50% of the wall thickness to be the point of failure[2]. This is justified if we consider that, as recession proceeds, the creep rate accelerates. By the time the thickness is only 50% of the starting thickness, the stress is doubled and if creep rates vary according to the Norton equation,

$$\dot{\varepsilon} = A\sigma^n \qquad (1)$$

where n the stress exponent, for instance n=3.5[3] and σ the stress, the strain rate would increase by a factor of 11 times. Considering lifetime is related to the creep rate, the expected lifetime is diminished at an accelerated rate. Several creep failure predictive equations are available. Larson-Miller and Monkman-Grant are the most common[4]. The Monkman-Grant equation is,

$$t_f = C\,\dot{\varepsilon}_s^{-M} \qquad (2)$$

[1] M. Van Roode and M. K. Ferber, "Long-Term Degradation of Ceramics for Gas Turbine Applications: ASME paper GT2007-27956," ASME Turbo Expo 2007: Power for Land, Sea and Air (2007).
[2] M. Van Roode and M. K. Ferber, "Long-Term Degradation of Ceramics for Gas Turbine Applications: ASME paper GT2007-27956," ASME Turbo Expo 2007: Power for Land, Sea and Air (2007)
[3] S. M. Wiederhorn, D. E. Roberts, , Tze-Jer Chuang, , and L. Chuck,, "Damage-Enhanced Creep in a Siliconized Silicon Carbide: Phenomenology," J Amer.Ceram.Soc., 71, 602-608 (1988).
[4] F. C. Monkman and N. J. Grant, "An Empirical Relationship between Rupture Life and Minimum Creep Rate in Creep-rupture Tests," Proceedings of the ASTM, 56, 593-(2007).

Considering *M=1.8*[5] the projected lifetime when the thickness was reduced to 50% would be ~ 75 times shorter than originally projected.

Improved creep resistant composites can be achieved either by using more creep resistant fibers such as Hi-Nicalon Type S (Nippon Carbon) and Tyranno SA (Ube Industries) as well as by a denser matrix. Melt infiltrated (MI) SiC matrix (molten Si) has improved the density of the matrix over CVI (chemical vapor infiltrated) however, in tests by Solar Turbines of EBC coated SiC-SiC composite liners, the service life of the two were equivalent[6]. More recently, combining MI, SiC particulate fillers and CVI has lead to panel densities of ~2.83 g/cm^3 or about 88% of the density of SiC[7], and creep strains as little as 0.05% are observed after 100 hrs at 1315ºC and 103 MPa. It remains to be seen whether significant improvements in lifetime will be achieved by these denser, creep resistant SiC-SiC composites.

B.2 Evolution of oxide-oxide CMCs: alternative to SiC-SiC CMCs

Oxide-oxide composites are showing great promise because of very much lower recession rates in long term combustor environments. On the other hand, the creep resistance of SiC fiber composites is much better in the temperature range of 1000-1400 ^{o}C. For instance, an oxide-oxide composite using woven Nextel 720 fibers and a polymer impregnated and pyrolyzed (PIP) alumina matrix after 100 hr at 1315 °C and 105 MPa in air, exhibited >0.2% creep strain. In contrast, under the same conditions SiC-SiC composite with a woven Hi Nicalon S SiC fiber and a SiC (CVI+slurry+Si) matrix only exhibited 0.05% strain[8]. The creep resistance of CMCs is generally dominated by the fiber. This is especially true of oxide-oxide composites where the lower density matrix does not contribute appreciably to creep resistance. Table I contains the temperature at which fibers can achieve <1% deformation in 1000 hrs at 69 MPa, which might be considered the maximum use temperature[9]

Table I: Maximum use temperature for oxide fibers (Wilson[9])

Property	Nextel 610	Nextel 650	Nextel 720
Composition	>99% Al_2O_3	89% Al_2O_3. 10% ZrO_2, 1% Y_2O_3	85% Al_2O_3, 15% SiO_2
Tensile Strength	33.3 GPa	2.8 GPa	2.1 GPa
Max. Use Temp.	1000º C	1080º C	1150º C

[5] H. G. Halverson, and W. A. Curtin, "Stress Rupture in Ceramic-Matrix Composites: Theory and Experiment", J. Amer. Ceram. Soc., 85, 6, 1350-1365 (2002)

[6] M. Van Roode, J. R. Price, J. Kimmel, N. Miriyala, D. Leroux, A. Fahme, and K. Smith, "Ceramic Matrix Composite Combustor Liners: A Summary of Field Evaluations: ASME Paper GT2005-68420," J.Eng.Gas Turbines & Power, 129, 1, 21-30 (2005).

[7] G. N. Morscher, and V. V Pujar, , "Creep and Stress-Strain Behavior after Creep for SiC Fiber Reinforced, Melt-Infiltrated SiC Matrix Composites," J Amer.Ceram.Soc., 89, 5, 1652-1658 (2006).

[8] J. A.DiCarlo, "High-Performance SiC/SiC Ceramic Composite Systems Developed for 1315 °C (2400 °F) Engine Components," (2003); G. N. Morscher, and V. V Pujar, , "Creep and Stress-Strain Behavior after Creep for SiC Fiber Reinforced, Melt-Infiltrated SiC Matrix Composites," J Amer. Ceram. Soc., 89, 5, 1652-1658 (2006).

[9] D. M. Wilson, "New High Temperature Oxide Fibers High Temperature Ceramic Matrix Composites," edit W. Krenkel, , R. Naslain, and H. Schneider, in High Temperature Ceramic Matrix Composites , pp. 3-13, Wiley, Darmstadt, Germany (2001).

To avoid excessive creep, thermal barrier coatings (TBCs) are applied to reduce the material's exposure temperature. These coatings, which are porous and thermally insulating, are designated as Friable Graded Insulation (FGI) because they erode with time. Considerable success has been achieved with this strategy. For instance, an Al_2O_3-Al_2O_3 composite annular combustor liner with FGI from COI Ceramics tested in a *Centaur®50S* engine accumulated ~25,400 hours before the test was shut down for examination of the liner. Since the coating thickness recedes with time, the temperature experienced by the composite rises with time. In the above test, some of the FGI remained even after 25,400 hours. The initial temperature experienced by the composite may be as low as 550º C. To allow the FGI to be effective, considerable back-side cooling is necessary, leading to reduced efficiency of the engine. This of course defeats the whole purpose since the ultimate goal is to obtain higher engine efficiency. Therefore, to improve efficiency, the back-side cooling will need to be reduced or even eliminated. Consequently, future composites with higher temperature capabilities need to be developed.

Several oxide fibers have been studied and tested to date. As observed from Table I the order of strengths is the reverse of the order of temperature capabilities. Nextel 610 is the least creep resistant because of its nanocrystalline grain size, which is also responsible for its high strength. Nextel 720 is designed with needle-like mullite grains (~0.5 μm); a material known to be very creep resistant because of its resistance to grain boundary sliding, but not as strong as the nanocrystalline alumina. For applications such as combustor liners, more important than the high room temperature strength is strength retention after high temperature exposure. After 100 hours of exposure, all three fibers are approximately of equal strength. Even more important is strength after exposure to both temperature and stress. In this case, the Nextel 720 fibers are much stronger[10].

The necessity of crack deflection at the matrix-fiber interface can either be achieved by coating the fibers with a weak coating, which is the case in virtually all the SiC-SiC composites, or by using a very porous matrix which is much less tough than the fiber, and will allow crack deflection. The latter approach was originally proposed by Tu[11] and is the approach used in most commercial prototype oxide-oxide composites today. Two oxide-oxide composites of this type are General Electric's (GE) GEN-IV and COI ceramics (COI), which both use an alumino-silicate matrix. The silica is added to bond alumina since shrinkage of an alumina matrix during sintering is difficult due to the constraint of volume change in a fiber framework. Because of volatilization, the silica present could limit the lifetime of these composites under high temperature exposure. Experimental versions of oxide-oxide composites containing only alumina or alumina YAG have been put forth. For instance, Levi et al[12] use a nano-particulate alumina to sinter/bind larger mullite particles. Several problems exist with the porous matrix approach. The major problem is sintering of the matrix to densities in excess of about 30% where the matrix is no longer sufficiently weak for crack deflection to occur. This would not be a

[10] D. M. Wilson, "New High Temperature Oxide Fibers High Temperature Ceramic Matrix Composites," edit W. Krenkel, , R. Naslain, and H. Schneider, in High Temperature Ceramic Matrix Composites , pp. 3-13, Wiley, Darmstadt, Germany (2001).

[11] W. C. Tu, F. F. Lange, and A. G. Evans, "Concept of a Damage Tolerant Ceramic Composite with "Strong" Interfaces," J Amer.Ceram.Soc., 79, 2, 417-424 (1996)

[12] C. G. Levi, F. Zok, J-Y Yang, M Mattoni, and J. P. A Loefvander, "Microstructural Design of Stable Porous Matrices for All-Oxide Ceramic Composites," Zeitschrift fur Metallkunde, 90, 12, 1037-1047 (1999).

problem if coated fibers were used. Also, welding of fibers without coatings creates a source of flaws[13].

A number of investigators have concluded that in the long run a YAG matrix is necessary, both because of its improved creep resistance and improved recession rate. In a burner rig test conducted at 1450 ^{o}C and v=100m/s gas flow velocity, Fritsch and Klemm [14] found a weight loss of 2.4 x 10^{-2} mg/cm^2/hr for Al_2O_3 compared to 2.1x10^{-3} mg/cm^2/hr for YAG, i.e. 10x decreased recession rate. The creep resistance of YAG is also an order of magnitude better than Al_2O_3 and the results of our Phase I study indicate that the creep resistance can be improved further by an order of magnitude by adding a small amount of La_2O_3 to the YAG.

C. Objectives

The overall technical objective of the program is to advance the state of the art in oxide/oxide CMCs through innovations in the matrix composition and structure. The ultimate goal is to have a material that has a life expectancy of 30,000 hours in gas turbine applications with temperatures in excess of 1200 ^{o}C. Specifically, the Phase I objectives were:

(i): To synthesize pure and doped YAG powder with nanometer-sized particles ;

(ii): To densify the doped and pure YAG powder using hot pressing and conventional sintering;

(iii): To measure the compressive creep rate of the compacts at elevated temperatures, and compare them to conventional materials;

(iv): Fabricate a fiber composite, using above mentioned powders.

We have accomplished the above mentioned objectives during the Phase I program and following are descriptions of Phase I experimental work.

D. Descriptions of Phase I Experimental Work

D.1 Synthesis of YAG and Doped-YAG powders

Pure YAG and Doped-YAG powders were synthesized using a solution method. We used aluminum nitrate nonahydrate, yttrium nitrate hexahydrate, and dopant nitrate as precursors for Al, Y and dopant respectively. The precursors were dissolved in distilled water. In a separate container, a 3 M NH_4OH solution was prepared. Subsequently, Al/Y/dopant solution was added to the NH_4OH solution using a peristaltic pump to precipitate Al – Y- dopant hydroxides. The precipitate was dried in an oven. The dried precipitates were heat-treated in air at 1000 ^{o}C, to transform them into YAG. For a typical experiment to produce 120 g of pure YAG, 379.16 g of $Al(NO_3)_3.9H_2O$ and 232.27 g of $Y(NO_3)_3.6H_2O$ were dissolved in 1 L of distilled water. Subsequently, 2.425 L of 3 M NH_4OH solution was prepared. After precipitation and heat treatment, 116 g of powder was obtained, which amounts to a yield of 96.7%.

---

[13] D. M. Wilson, "Statistical Tensile Strength of Nextel 610 and Nextel 720 Fibers," J. Mater. Sci., 32, 2535-42 (1997).

[14] M. Fritsche and H Klemm, Ceramic Engineering and Science Proceedings, **27** [3], Advanced Cermic Coatings and Interfaces, p.149-159 (2006)

Table II is a list of all the powder lots that were synthesized in the Phase I program. In the case of YAG-Lot E powder, pure YAG powder was synthesized initially, after which dopant nitrate was added to the powder to coat the YAG particles with dopant oxide. This powder is referred as “External” to contrast other doped powders where all the precursors were mixed in the first stage of synthesis. As synthesized samples were analyzed using X-ray diffraction, SEM and single point BET (for surface area). Table I shows different types of powders prepared during the Phase I program. Note that the surface area values for the YAG particles in Table II is substantially more than that of commercial micron-sized powders, which tend to be in the 2-5 m^2/g.

Table II: List of different types of powder synthesized during Phase I

Sample ID	**Dopant-oxide (%)**	**Addition**	**Surface Area (m^2/g)**
YAG-Lot A	0	-	17.3
YAG-Lot B	0.1	Internal	17.6
YAG-Lot C	0.2	Internal	14.6
YAG-Lot D	0.3	Internal	18.8
YAG-Lot E	0.1	External	17.3

Figure 1 shows the X-ray diffraction pattern of as-synthesized powders, which confirms the formation of phase pure YAG. The presence of dopant cannot be detected from X-ray diffraction due to its low sensitivity. However, we measured the lattice parameters to observe any variation due to the presence of dopant ions in the matrix. Due to the ionic radius difference between dopant ion and the other cations in YAG, the lattice parameter can be expected to increase with increasing concentration of dopant ions. Figure 2 shows the variation in the lattice parameter with change in the concentration of dopant ion. As expected, the lattice parameter increases with increasing concentration of dopant ion. When the same powder was heat treated at 1500 ^oC for four hours, the lattice parameter decreased for all the powders to the same level (within the error bar), indicating that dopant ions have segregated out to the grain boundaries. This significant finding correlates exceptionally well to the creep properties of doped YAG.

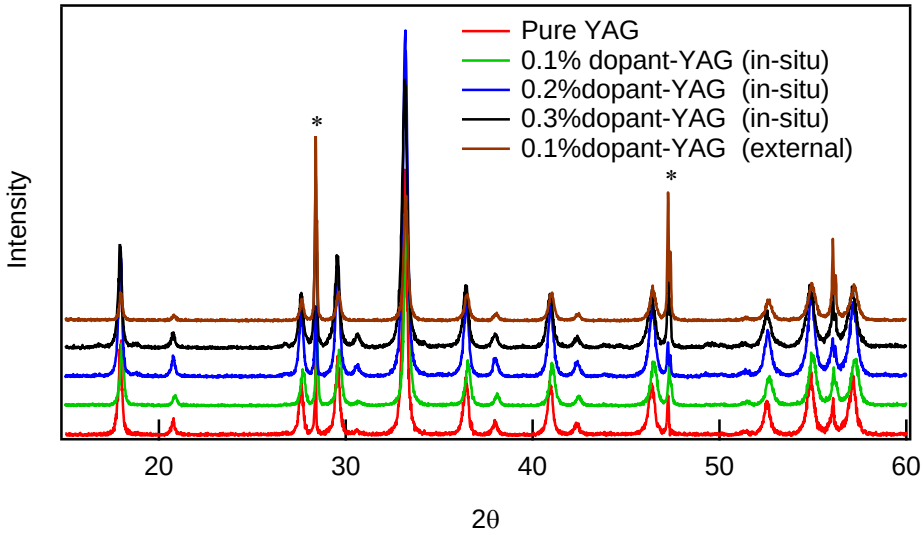

Figure 1: X-ray diffraction pattern of different types of powders synthesized during Phase I.

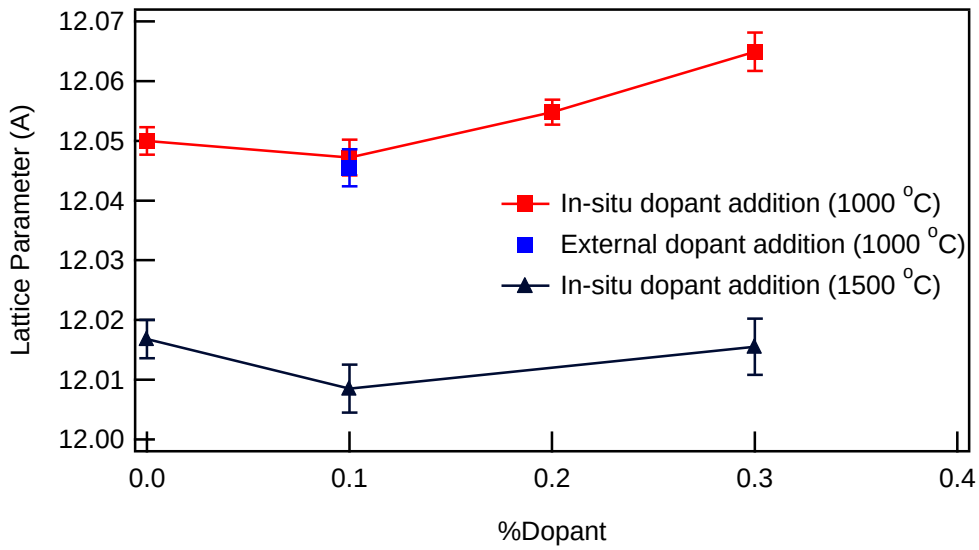

Figure 2: Variation of lattice parameters with dopant concentration.

Figure 3 shows SEM micrographs of as-synthesized powders. As can be observed from the micrographs, the size of some of the aggregates is as much as 30 µm. We deliberately did not mill the powder to reduce the aggregate size, because the intention was to transform these aggregates into larger grains, which would be difficult to achieve if the aggregates were small. As mentioned before, sintering YAG is particularly difficult, with Y^{3+} cation being the slowest moving species, as was shown by M. Jimenez-Melendo and H. Haneda[15].

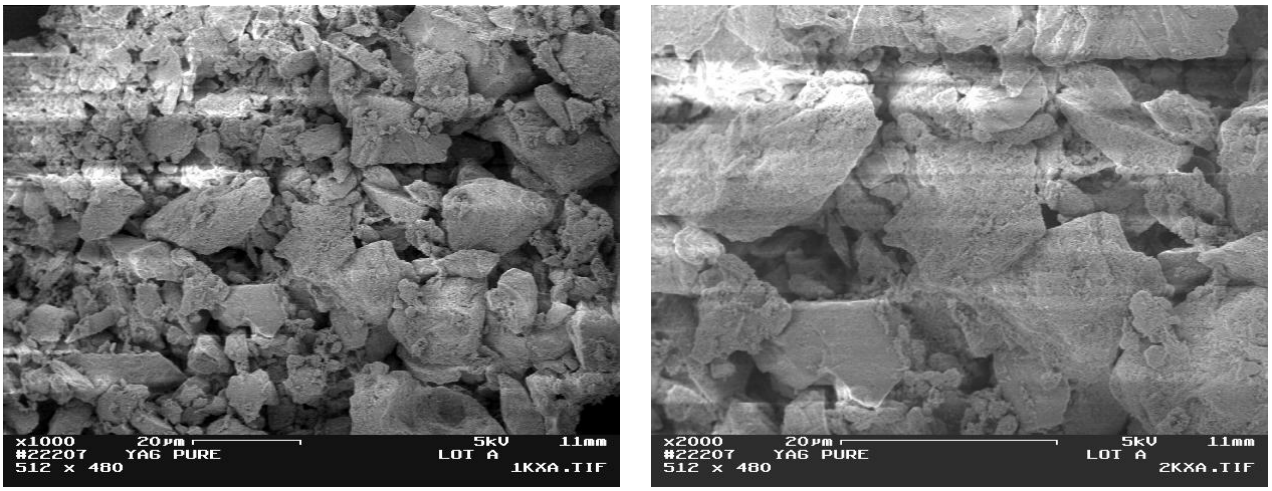

Figure 3: SEM micrographs of powders used for sintering.

D.2 Compaction of YAG powder for pressure-less sintering

During the initial stages of the Phase I program, we decided to sinter the YAG powder using pressure-less sintering. The goal was to achieve near theoretical density so that the creep rate

[15] Manuel Jimenez-Melendo and Hajime Haneda, Ytterbium cation diffusion in yttrium aluminum garnet – implications for creep mechanisms, *J. Am. Ceram. Soc.,* 84 [10] 2356-60 (2001).

can be determined accurately. The powders were mixed with 3 wt% poly (vinyl butyral) (PVB), which acts as a binder. This was achieved by initially dissolving PVB in ethanol, and subsequently adding powder, while agitating the mixture using a magnetic stirrer. The ethanol was evaporated using a rotovapor, and the powder was compacted using a 0.5 cm die. As-compacted samples were typically 0.55-0.72 cm in height. Some of the samples were also cold isostatically pressed after compaction at a pressure of ~200 MPa. The samples were then heat treated at 700 ^{o}C for 2 hours in O_2 atmosphere to remove the binder. The relative green density of the samples after binder burnout was ~45-50 % of the theoretical density.

Some of the samples were sintered in a tube furnace at temperatures between 1300 ^{o}C and 1500 ^{o}C in air, and the rest of the samples were sintered at 1740 ^{o}C in a vacuum furnace. The maximum density was 86.6 % for the sample sintered at 1740 ^{o}C for 2 hours in vacuum. The density values are listed in Table III. Since we wanted to get fully dense samples so as to be able to obtain reliable and accurate creep measurements, we decided to hot-press the powders to achieve higher densities.

Table III: Relative densities of YAG and doped-YAG samples after pressureless sintering.

Sample ID	RE-oxide (%)	CIPed	Atm.	Temp. (^{o}C)	Time (Hours)	Relative Density (%)
YAG-Pure-1	0	No	Air	1300	2	50.6
YAG-0.1%dopant-1	0.1	No	Air	1300	2	49.3
YAG-Pure-2	0	No	Air	1500	3	55.7
YAG-0.1%dopant-2	0.1	No	Air	1500	3	55.7
YAG-Pure-3	0	Yes	Vacuum	1740	2	79.4
YAG-0.1%dopant-3	0.1	Yes	Vacuum	1740	2	86.6

D.3 Densification of YAG powder using hot-pressing

The powders were compacted and hot-pressed at a company called TA&T. The powders were hot-pressed in a 2" diameter graphite die. Grafoil was used as a barrier between the YAG powder and graphite ram. The powders were pressed in argon atmosphere at 1700 ^{o}C and 24 MPa for 4 hours. The hot pressed discs were intact, but slightly dark in color due to O_2 deficiency. The discs were heat treated in air at 1000 ^{o}C to oxidize the samples before further characterization. Table IV shows the relative densities of the discs after heat treatment. The discs were 95-98 % dense, which is a reasonable density to perform precise creep rate study.

Table IV: Relative densities of hot-pressed discs

Sample ID	RE-oxide(%)	Temperature (^{o}C)	Time (Minutes)	Pressure (MPa)	Relative density (%)
YAG-Lot A	0	1700	120	24	95
YAG-Lot B	0.1	1700	120	24	98
YAG-Lot C	0.2	1700	120	24	96
YAG-Lot D	0.3	1700	120	24	97
YAG-Lot E	0.1 (External)	1700	120	24	98

Figure 4 shows SEM micrographs of a sintered pure YAG sample at various magnifications and different regions of the sample. The micrographs show exaggerated grain growth in some regions where grains have grown to >20 μm. This is most likely a consequence of starting with highly aggregated but high surface area powders. As described below, these grains have a profound effect on the creep rate, and might as well be the rate controlling grains. Figure 5 shows the micrograph of a (0.3%dopant) –YAG sample, where the microstructure is quite similar.

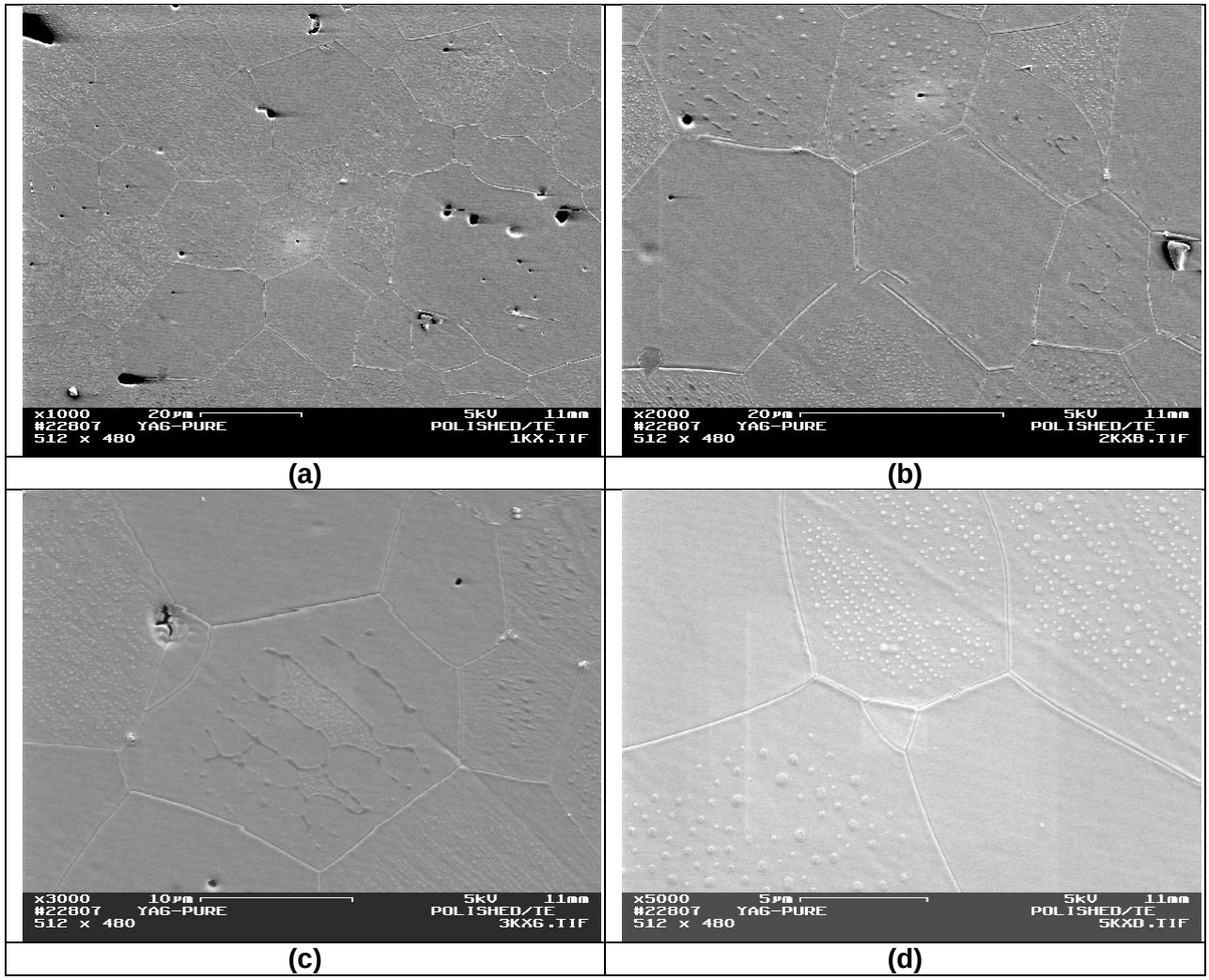

Figure 4: SEM micrograph of hot-pressed and polished surface of pure-YAG sample used for creep test.

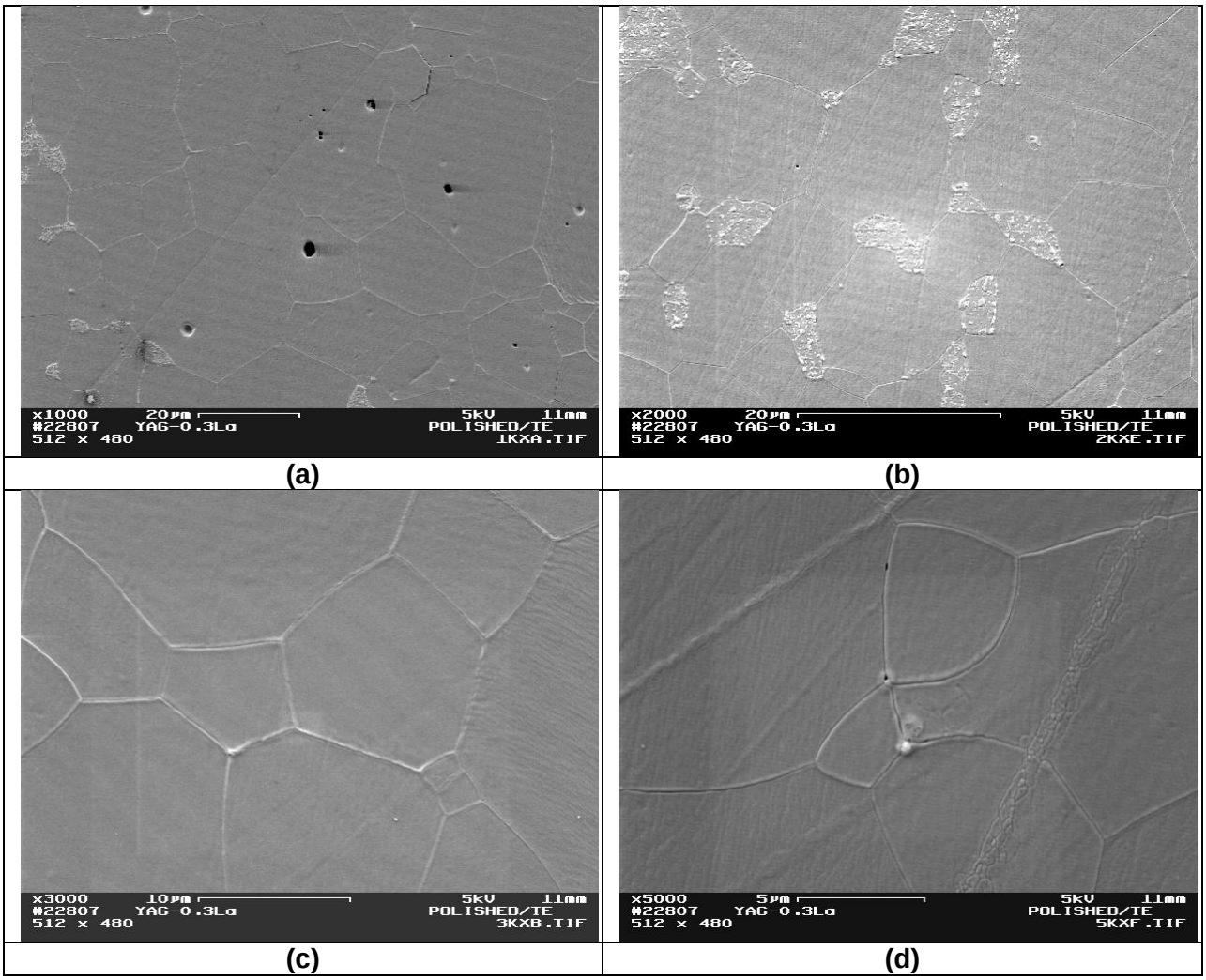

Figure 5: SEM micrograph of hot-pressed and polished surface of (0.3%dopant)-YAG sample used for creep test.

Figure 6 shows the grain size distribution in hot-pressed pure YAG samples. The intercept method was used to determine the grain size. The average grain size was ~9 µm. A similar type of grain structure was observed for 0.3% dopant-YAG.

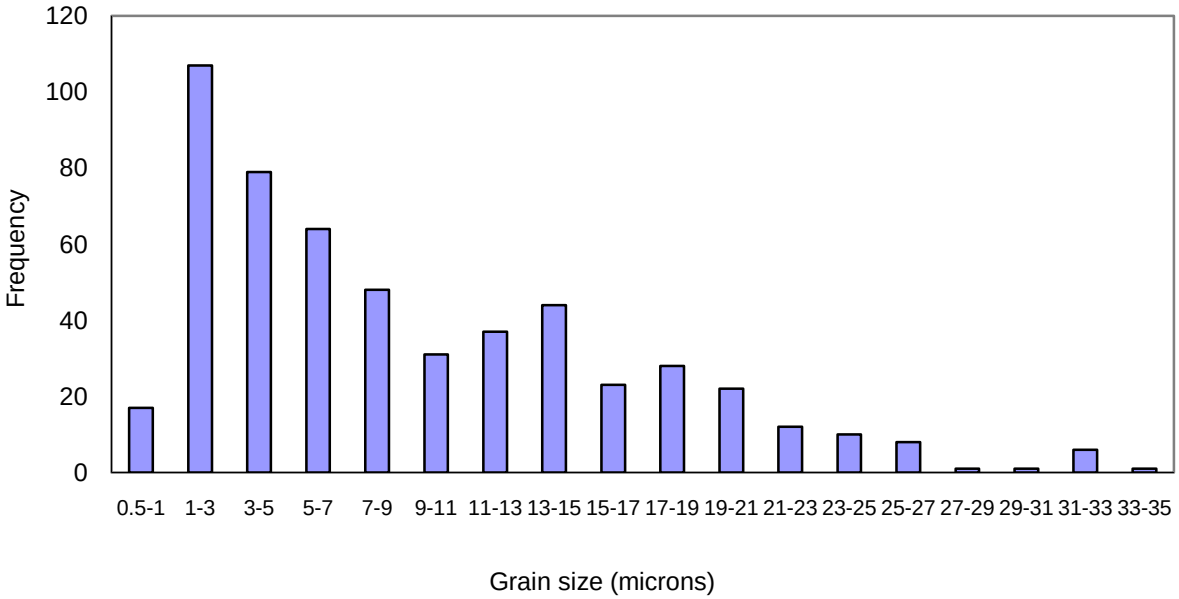

Figure 6: Grain size distribution in a hot-pressed YAG sample, which was used for creep measurements.

Since in a practical CMC, the processing temperature is not likely to be more than 1300 ^{o}C due to the potential for damaging the fibers, a selected powder sample was hot pressed at 1300 ^{o}C for 4 hours at a pressure of 24 MPa. The sintered density was ~ 70%. Figure 7 shows an SEM micrograph of a pure YAG sample processed at 1300 ^{o}C.

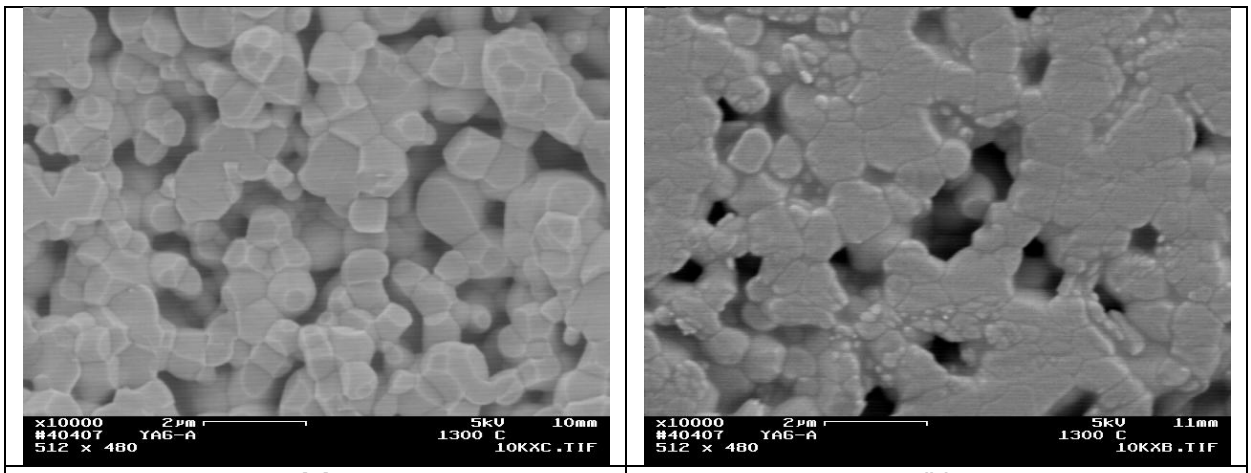

(a) (b)

Figure 7: SEM micrograph of hot-pressed pure YAG sample – processed at 1300 ^{o}C **(a)** fractured surface; **(b)** polished and thermally etched surface.

D.4 Creep measurement of sintered YAG samples

In order to perform the creep studies, we machined the discs into cubes with dimensions of 4×4×4 mm. Figure 8 shows a photograph of a typical sample used for creep properties measurement.

Figure 8: Photograph of a typical sample used for creep measurements (4x4x4 mm).

Creep measurements were performed in compression on hot pressed YAG and YAG + 0.3% dopant at temperatures between 1300ºC and 1390ºC. Measurements were performed on specimens ground flat to approximately ±5 μm. Tests were performed in compression using an Instron Electromechanical Actuator and SiC push rods. Each test was performed at a constant stress without changing stress during the test. For creep rates $<10^{-8}$ sec^{-1}, drift was too great and so rates were determined from the change in length of the specimen measured with a micrometer divided by the total time. It was estimated from the degree of primary creep (faster initial rate) shown in other tests that this overestimated the creep rate by as much as a factor of two.

Creep curves for the two different compositions, pure YAG and YAG + 0.3% dopant are shown in Figure 9. It is clear that the addition of 0.3% dopant both greatly reduces the creep rate and increases the time to failure. The primary stage may be due to specimens being flat only to about ±5 μm. In most creep tests the creep rates were quite linear over an appreciable portion of the curve and the slope was taken as the steady state rate. In all cases, the minimum creep rate is reported. Several tests were not terminated during the tertiary creep stage and specimens were completely reduced to rubble by the time the creep tests were complete. Specimens with more parallel faces did not exhibit as great a degree of tertiary creep nor were they reduced to rubble during the creep test.

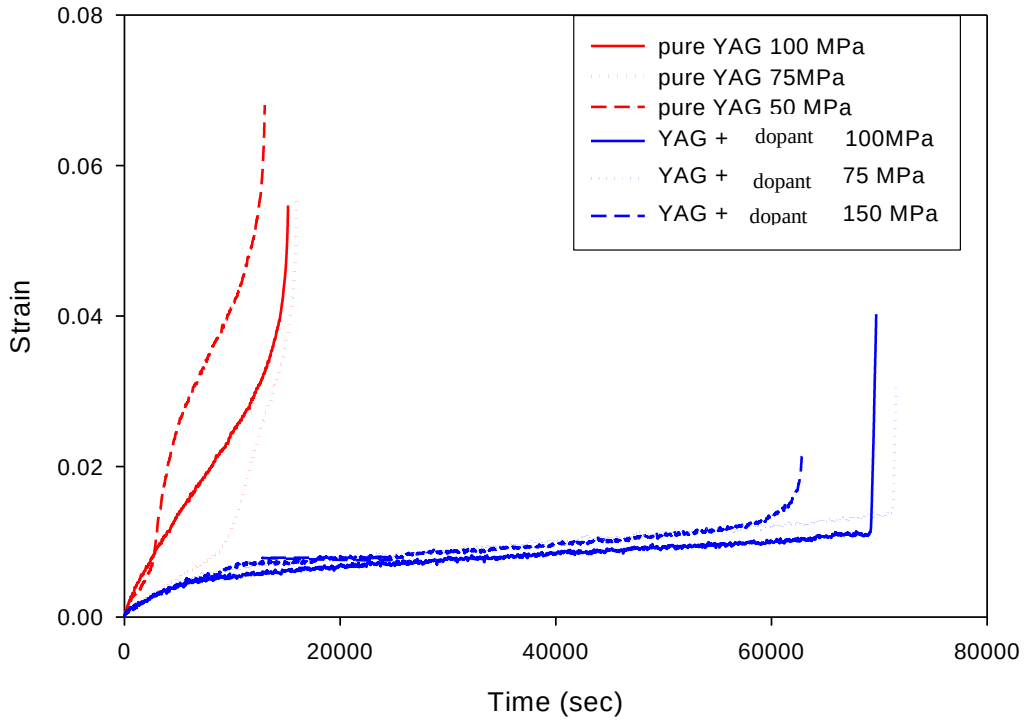

Figure 9: Typical creep curves for YAG (grains size 7 ± 2.4 μm) and YAG + 0.3% dopant (grain size 8.8 ±2.6 μm) at 1390ºC.

Figure 10 compares the steady state creep rates vs. stress at 1390ºC between the two compositions. The approximately one order of magnitude improvement in creep resistance by adding 0.3% dopant is too high to originate from merely decreased lattice diffusivity since dopant ions substituting for Al^{+3} in the lattice would produce no additional vacancies. In the Phase I proposal it was proposed that the addition of dopant in small amounts might greatly reduce the creep rate. The particular dopant was chosen because of its large ionic radius, in anticipation that dopant ions would segregate to the grain boundary and reduce the grain boundary diffusion rate. French et al and others[16] showed that the creep rate of Al_2O_3 was decreased by approximately two orders of magnitude by adding large ions, mostly rare earth ions. XRD results in Figure 2 indicate that dopant is not in solid solution within the lattice after annealing at 1500ºC and so it must either be in a second phase or segregated to the grain boundaries in solid solution. It has been shown experimentally and theoretically that the formation of a small amount of second phase will not affect the creep rate[17] significantly and so it is contended that the large dopant ions segregate to the grain boundaries in solution. Harmer

[16]. D. French, Yongnian Zhao, , M. P. Harmer, H. M. Chan, , and G. A. Miller, "Creep of Duplex Microstructures," Journal of the American Ceramic Society, 77, 11, 2857-2865 (1994); Yan-Zun Li, C. Wang, H. M. Chan, J. M. Rickman, and M. P. Harmer, "Codoping of Alumina to Enhance Creep Resistance," J Amer.Ceram.Soc., 83, 6, 1497-1504 (1999).

[17] Yan-Zun Li, C. Wang, H. M. Chan, J. M. Rickman, and M. P. Harmer, "Codoping of Alumina to Enhance Creep Resistance," J Amer.Ceram.Soc., 83, 6, 1497-1504 (1999).

and Chan's group[18] at Lehigh University showed that when large ions such as Y^{+3} are added to Al_2O_3 that the larger ion together with the small Al^{+3} ions (0.067 nm) and oxygen at the grain boundary form a more densely packed grain boundary with less free volume leading to the decrease in the grain boundary diffusion rate[38]. Since in YAG there is a combination of the small Al^{+3} ion and the larger Y^{+3} ion (0.104 nm), it was uncertain at the time of the writing of the Phase I proposal whether the same effect would be observed. Fortunately it was.

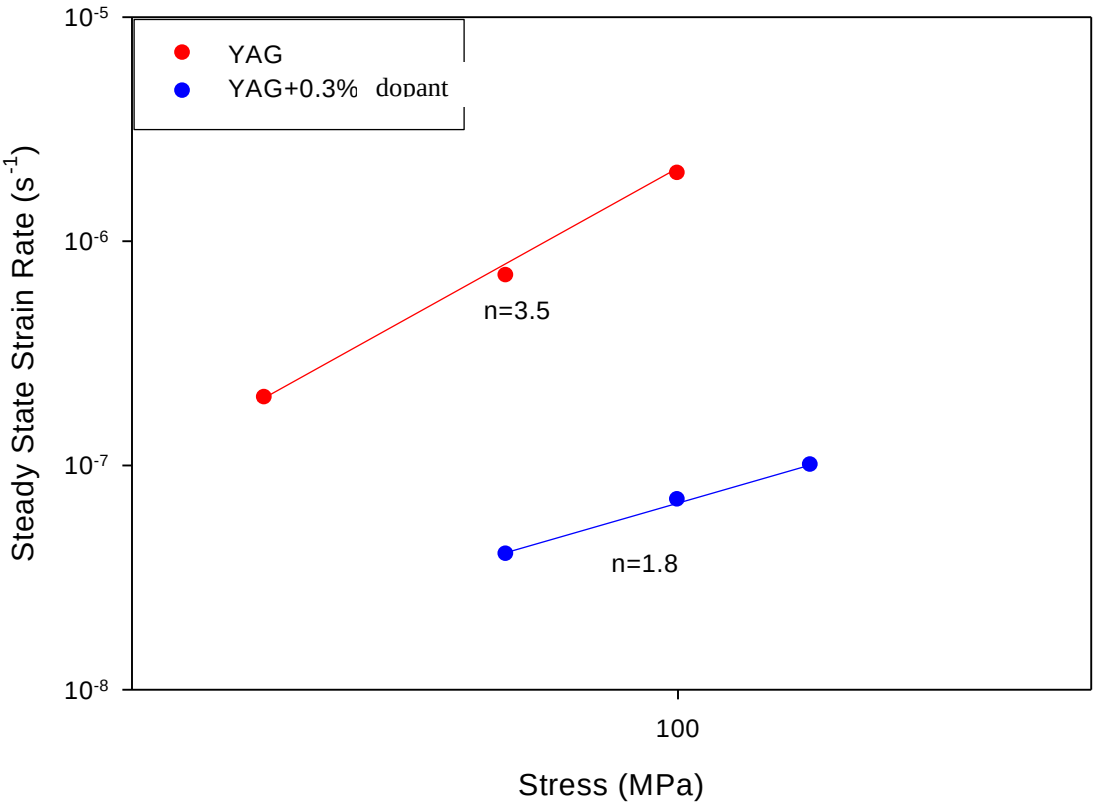

Figure 10: Comparison of steady state strain rates between YAG and YAG + 0.3% dopant at 1390ºC.

Figure 11 compares the creep rates from this work with those of Al_2O_3 and YAG from the work of French et al[19]. Differences in the creep rate of YAG were presumably due to grain size. By considering the grain size of their work compared to ours, grain size exponent, *p*, in the equation $\dot{\varepsilon} = A'\sigma^n d^{-p}$ would be *p=2.5* which is in line with the Nabarro-Herring and Coble creep predictions. Creep rates also depend on the presence of exaggerated grain growth. The high p likely comes from the presence of exaggerated grain growth in our specimens.

[18] C. M. Wang, H. M. Cargill III, H. M. Chan, and M. P. Harmer, "Structure of Y and Z Segregated Grain Boundaries in Al2O3," Interface Science, 8, 243-255 (2000).

[19] J. D. French, Yongnian Zhao, , M. P. Harmer, H. M. Chan, , and G. A. Miller, "Creep of Duplex Microstructures," Journal of the American Ceramic Society, 77, 11, 2857-2865 (1994); L. Clarisse, R. Baddi, A. Bataille, J. Crampon, R. Duclos, and J. Vicens, "Superplastic Deformation Mechanisms during Creep of Alumina-Zirconia Composites," Acta Materialia, 45, 9, 3843-3853 (1997)

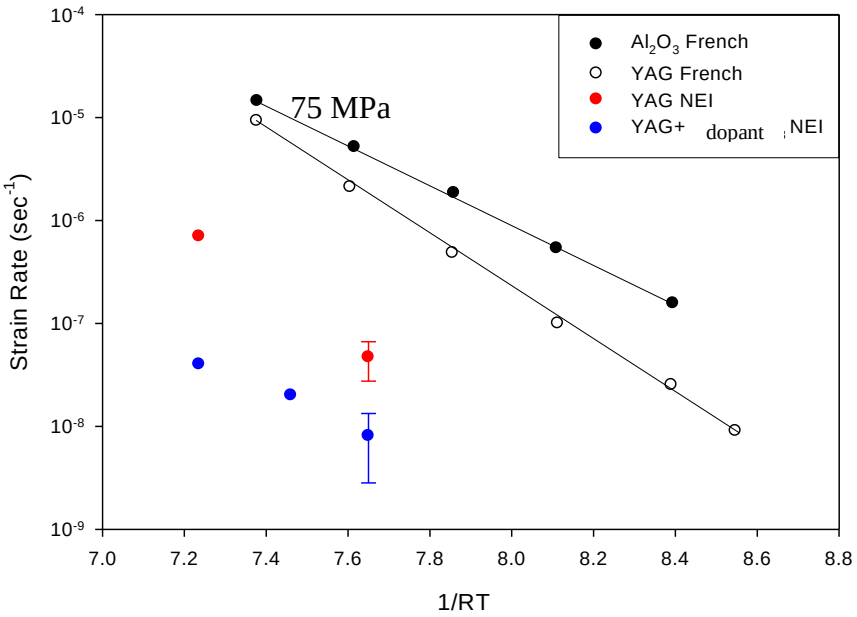

Figure 11: Comparison of creep rates with creep results for Al_2O_3 and YAG of French et al[40] with NEI Phase I results for YAG and YAG + 0.3% dopant.

Figure 12 compares the creep rates at 1100ºC of all the 3M Nextel fibers as well as experimental Al_2O_3-YAG fibers. The most creep resistant fiber is the Nextel 720 Al_2O_3-mullite fiber. In comparison, the creep resistance of the YAG + 0.3% dopant extrapolated to 1100º C is approximately 1 ½ orders of magnitude more than the Nextel 720 fiber, showing that the Phase effort has been successful in producing a significantly more creep resistant matrix material. Besides composition considerations, the high creep resistance of the YAG + 0.3% dopant comes from the 8.8 μm grain size. If we wish to maintain a matrix that is more creep resistant than the Nextel 720 fiber, there is still some latitude with grain size. If for instance, by fabricating the YAG + 0.3% dopant at 1300ºC, the grain size were only 3 μm the creep rate would still be a factor of five lower than the Nextel 720.

Even though we have demonstrated a method to achieve high densities at the upper limit of processing the composite, we are likely to attain about 80% theoretical matrix density. Langdon[20] has proposed a porosity correction for creep rate which has successfully been used to relate creep rates of porous ceramics to dense ones. The equation is

$$\frac{\dot{\varepsilon}_{porous}}{\dot{\varepsilon}_{dense}} = \frac{\left\{1+\beta P \Big/ \left[1-(\beta+1)P\right]\right\}^{1-n}}{\left(1-P^{2/3}\right)^{n}} \qquad (6)$$

Where P is the fraction of porosity, n is the stress exponent and β is a constant, ~4. Considering a stress exponent, $n=2$, the creep rate correction is 2.3. Considering the above correction for grain size and the porosity correction, this still leaves an approximately one half order of magnitude more creep resistance than the Nextel fiber.

[20] T. G. Langdon, "Dependence of Creep Rate on Porosity," J. Amer. Ceram. Soc., 55, 12, 630-634 (1972).

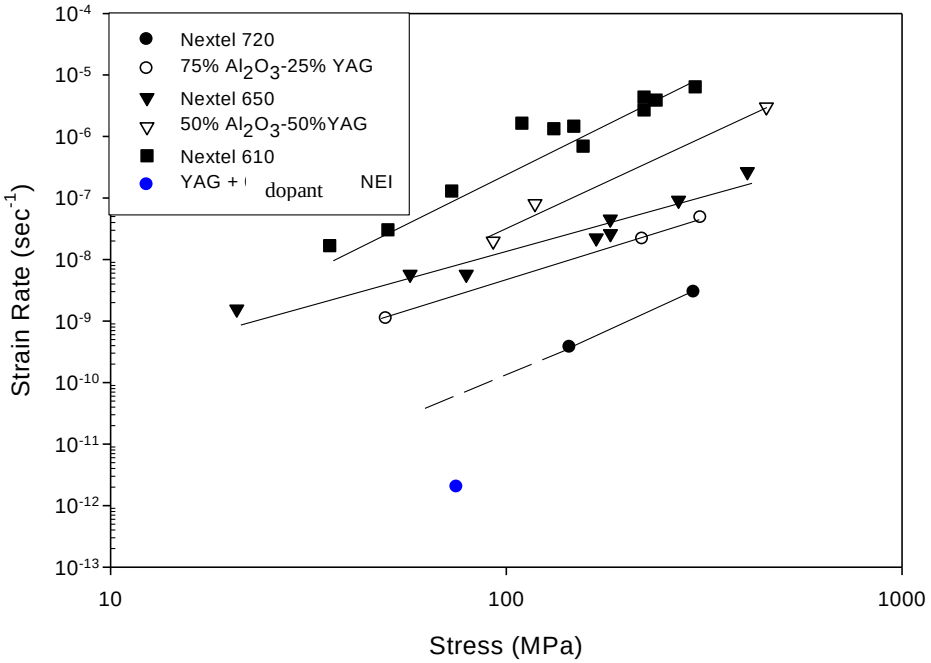

Figure 12: Comparison of creep rates between the various Nextel fibers and the creep rate of the YAG + 0.3%dopant.

Figure 13 shows the micrographs of the polished and fractured surface of pure YAG, after creep testing. The samples were thermally etched prior to microscopic analysis. The formation of cavities at the grain boundaries, due to diffusion of vacancies, can be observed in the micrographs of the fractured surface. A similar behavior was observed in the case of 0.3 % dopant-YAG composite (Figure 14). One significant difference between the fracture of pure YAG and doped YAG was that fracture of pure YAG was primarily transgranular, while the fracture of doped YAG was intergranular. It is likely related to the presence of dopant at the grain boundaries.

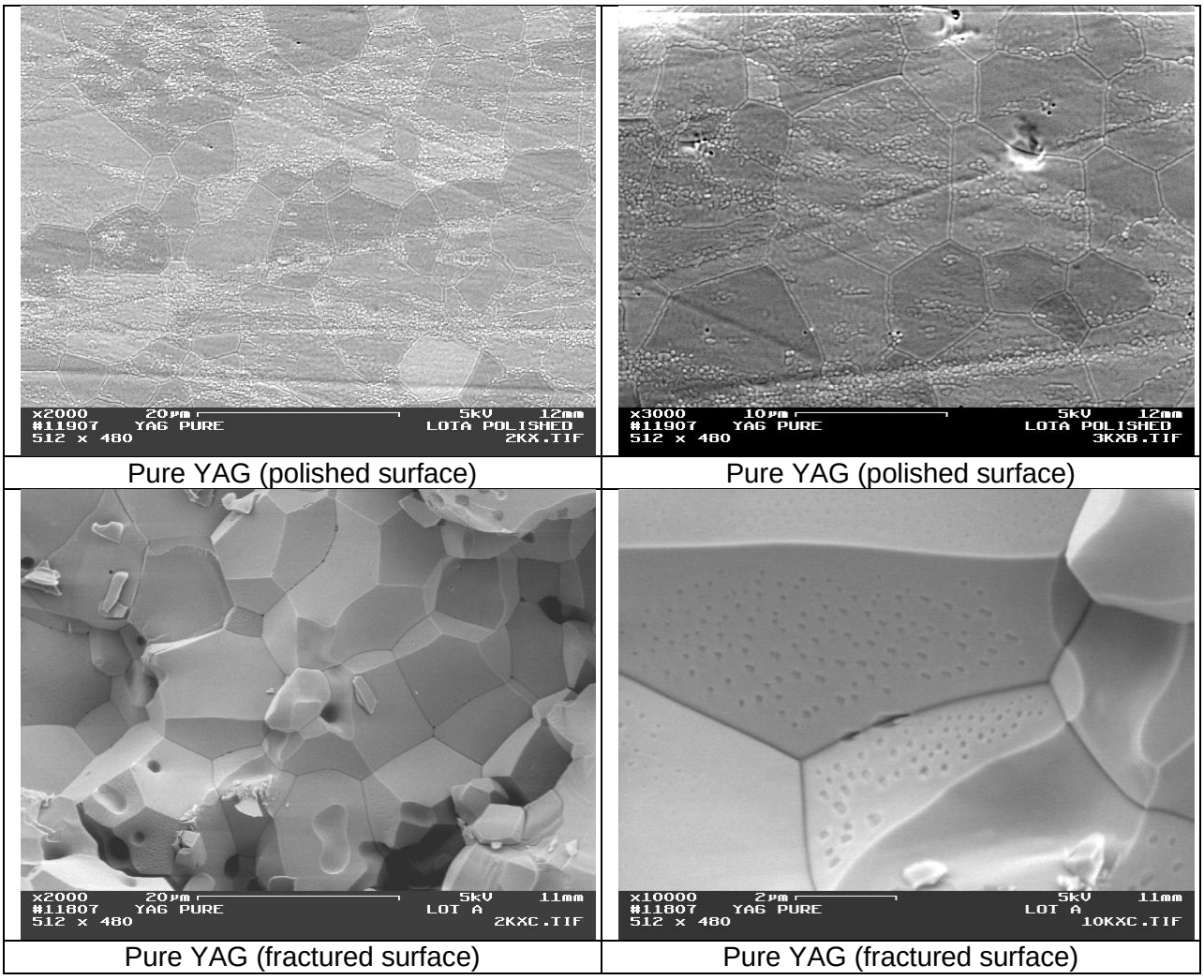

Pure YAG (polished surface)	Pure YAG (polished surface)
Pure YAG (fractured surface)	Pure YAG (fractured surface)

Figure 13: Polished and fractured surface of pure YAG after creep testing.

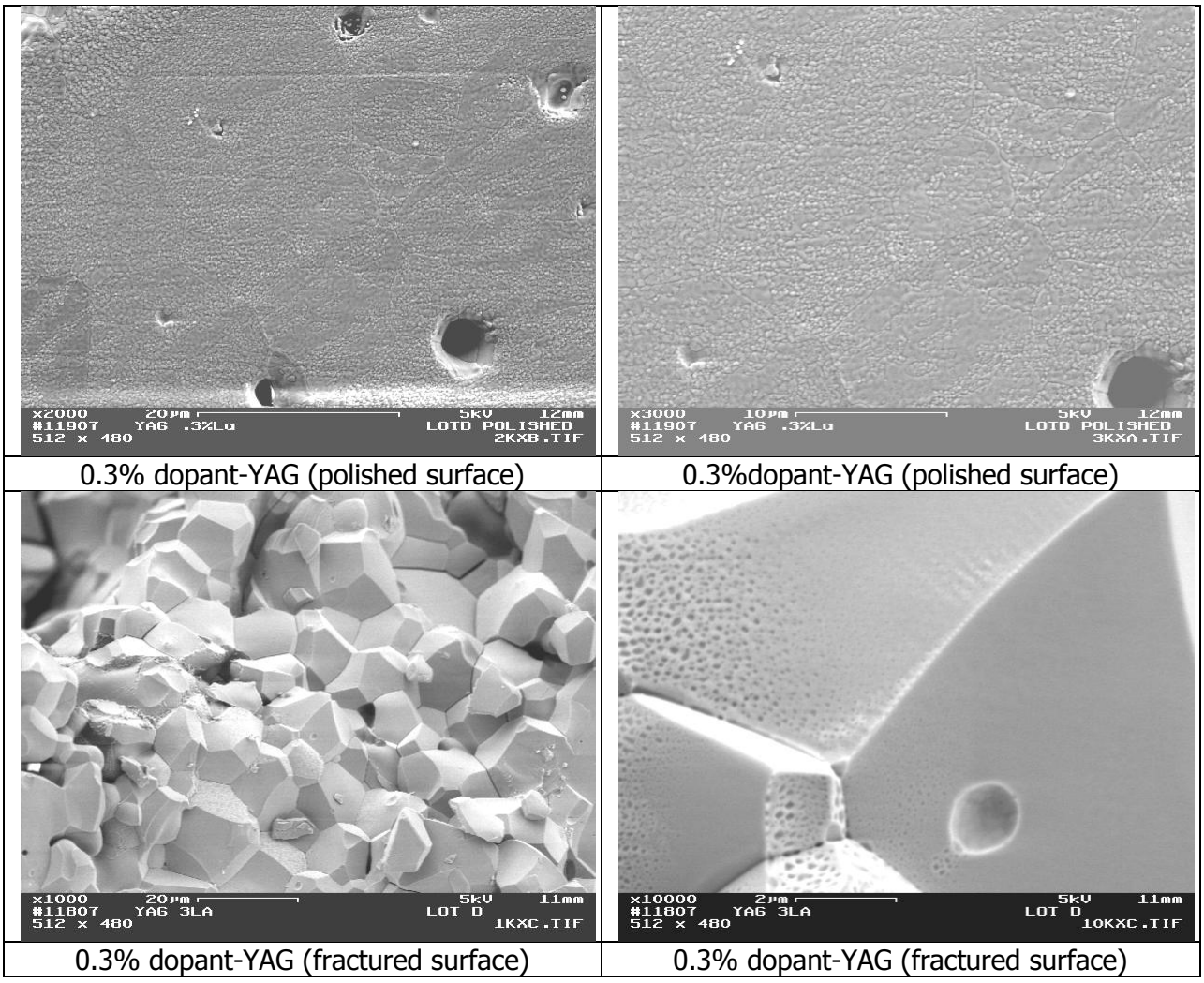

0.3% dopant-YAG (polished surface)	0.3%dopant-YAG (polished surface)
0.3% dopant-YAG (fractured surface)	0.3% dopant-YAG (fractured surface)

Figure 14: Polished and fractured surface of 0.3% dopant-YAG after creep testing.

D.5 Comparison between densification rates of commercial micron-sized YAG and NEI's nanoparticulate YAG

In order to compare the rates of densification of commercially available micron-sized YAG (S.A = 2.4 m^2/g) and NEI's nano-sized YAG, we measured the change in the length of cylindrical samples of commercial YAG and NEI's YAG, with temperature using a dilatometer. The measurements were performed from 60 ^oC to 1400 ^oC. Figure 15 shows the percent linear change in the dimension of the sample with temperature. The onset of densification in the case of nano-sized powder YAG was at ~1000 ^oC, while the onset of densification in the case of micron-sized powder YAG was ~1180 ^oC. The linear change was ~0.1% in the case of micron-sized powder sample, while it was ~2.5% in the case of nano-sized powder sample. This demonstrates that the densification rate of nano-sized powder is significantly higher than micro-sized powder, which is an important factor in achieving high final densities in CMCs at relatively low temperature.

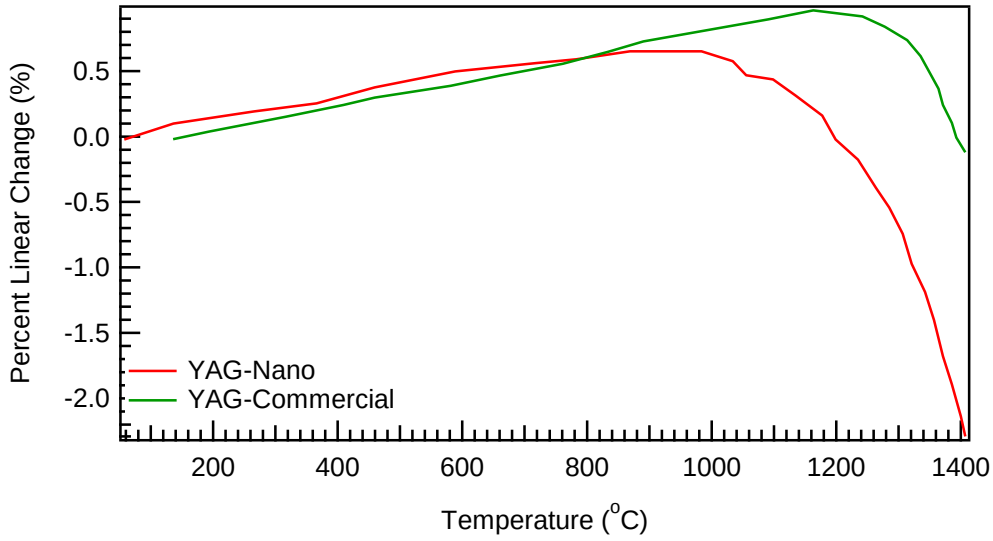

Figure 15: Linear percentage change vs. temperature for samples fabricated from micron-size YAG and nano-sized YAG powder.

D.6 Fabrication of CMC coupons

Preliminary studies were performed to synthesize fiber-matrix composites. A Nextel 720 fiber mat was used for the study. Two types of Nextel 720 fiber mats were used: Denier -1500 and Denier-3000. The fiber mats were initially de-sized to remove the organic coatings from the surface. This was achieved by heat treating the as received fiber mat at 600 ^{o}C for 1 hour in air. The color of the mat changed from green to off-white after heat treatment. Figure 16 shows a photograph of the fiber mat after heat-treatment.

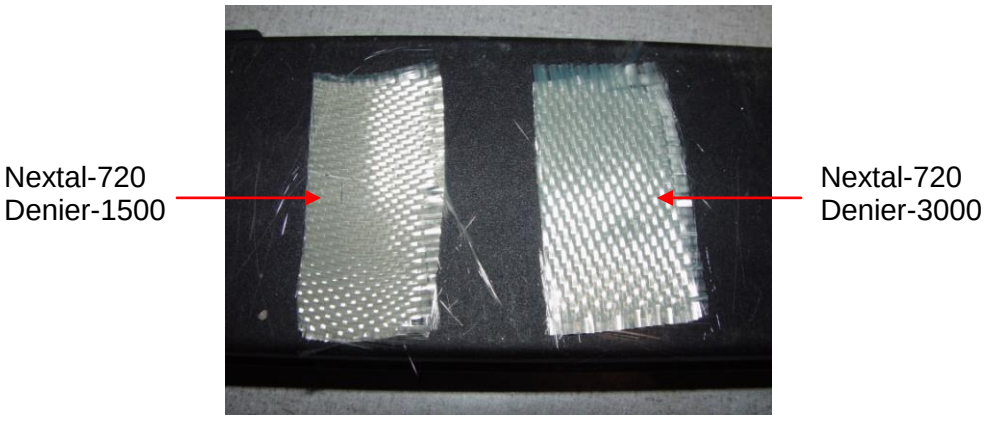

Figure 16: Photograph of Nextel-720 fibers mat after de-sizing.

The slurry of nano-sized YAG powder was prepared by first dissolving 1.5 % Darvan-C in water. Darvan-C acts as a dispersant for YAG nanoparticles. Subsequently, YAG powder was added to the solution, followed by addition of milling media (2 mm zirconia ball). A 20 vol% slurry was prepared for infiltrating the fiber mat. The slurry was milled for 24 hours. The viscosity of the slurry was reasonably low, so that it could be used easily for infiltration.

Four types of fiber mats were prepared for infiltration. The first two mats were heat-treated Denier-1500 and 3000, while the other two mats were heat-treated and soaked in 1.5 wt% Darvan-C prior to infiltration. The infiltration was performed by initially placing the samples in a three neck flask connected to a vacuum pump. Subsequently, a vacuum was generated in the flask, followed by the addition of the slurry using a syringe. Finally, the vacuum pump was disconnected and air was introduced into the flask, to apply external pressure. The sample was removed from the flask after infiltration, and dried in air, followed by sintering at 1300^{o}C for 4 hours. The sintered mat was infiltrated with YAG particles, followed by sintering. Figure 17 shows the mats after sintering. The mats were observed to be intact after infiltration and heat treatment.

Figure 17: Photographs of the CMCs after sintering.

E. Summary of Phase I Accomplishments

In Phase I, we demonstrated that the addition of a dopant, in YAG matrix, can significantly reduce the creep rate of YAG. Specifically, we have

(i) Synthesized doped and undoped aggregated YAG powder, with nanometer size particles;

(ii) Reduced the creep rate of YAG an order of magnitude using the dopant;

(iii) Determined the scientific reasons behind the reduction of creep rate;

(iv) Fabricated ceramic matrix composite using Nextel 720 fiber, and YAG powder.